

13. Scalapino, D. J. in *Superconductivity* (ed. Parks, R. D.) 449 (Marcel Dekker, New York, 1969)
14. Puchkov, A. V., Basov, D. N. & Timusk, T. The pseudogap state in high T_c superconductors: An infrared study. *J. Phys. Condens. Matter* **8**, 10049–10082 (1996).
15. Feng, D. L. *et al.* Bilayer splitting in the electronic structure of heavily overdoped $\text{Bi}_2\text{Sr}_2\text{CaCu}_2\text{O}_{8+\delta}$. *Phys. Rev. Lett.* **86**, 5550–5553 (2001).
16. Chuang, Y.-D. *et al.* Doubling of the bands in overdoped $\text{Bi}_2\text{Sr}_2\text{CaCu}_2\text{O}_{8+\delta}$ —probable evidence for c-axis bilayer coupling. Preprint cond-mat/0102386 at (<http://xxx.lanl.gov>) (2000).
17. Campuzano, J. C. *et al.* Electronic spectra and their relation to the (π, π) collective mode in high- T_c superconductors. *Phys. Rev. Lett.* **83**, 3709–3712 (1999).
18. Varma, C. M., Littlewood, P. B., Schmitt-Rink, S., Abrahams, E. & Ruckenstein, A. E. Phenomenology of the normal state of Cu-O high-temperature superconductors. *Phys. Rev. Lett.* **63**, 1996–1999 (1989).
19. Johnson, P. D. *et al.* On the doping and temperature dependence of the mass enhancement observed in the cuprate Bi2212 . Preprint cond-mat/0102260 at (<http://xxx.lanl.gov>) (2001).
20. Fong, H. F. *et al.* Polarized and unpolarized neutron scattering study of the dynamic spin susceptibility in $\text{YBa}_2\text{Cu}_3\text{O}_7$. *Phys. Rev. B* **54**, 6708–6720 (1996).
21. Carbotte, J. P. *et al.* Coupling strength of charge carriers to spin fluctuations in high-temperature superconductors. *Nature* **401**, 354–356 (1996).
22. Takagi, H. *et al.* Systematic evolution of temperature-dependent resistivity in $\text{La}_{2-x}\text{Sr}_x\text{CuO}_4$. *Phys. Rev. Lett.* **69**, 2975–2978 (1992).
23. Allen, P. B. Anomalous versus conventional low energy properties of cuprate superconductors. *Comments Condens. Matter Phys.* **15**, 327–353 (1992).
24. Gunnarsson, O. Superconductivity in fullerenes. *Rev. Mod. Phys.* **69**, 575–606 (1997).
25. Batlogg, B. *et al.* Normal-state phase-diagram of $(\text{La}, \text{Sr})_2\text{CuO}_4$ from charge and spin dynamics. *Physica C* **235**, 130–133 (1994).
26. Kubic, M. L. Interplay of electron-phonon interaction and strong correlations: the possible way to high-temperature superconductivity. *Phys. Rep.* **338**, 1–264 (2000).
27. Renner, C. H. *et al.* Pseudogap precursor of the superconducting gap in under- and overdoped $\text{Bi}_2\text{Sr}_2\text{CaCu}_2\text{O}_8$. *Phys. Rev. Lett.* **80**, 149–152 (1998); Observation of the low temperature pseudogap in the vortex core of $\text{Bi}_2\text{Sr}_2\text{CaCu}_2\text{O}_8$. *Phys. Rev. Lett.* **80**, 3606–3609 (1998).
28. Cren, T. *et al.* Influence of disorder on the local density of states in high- T_c superconducting thin films. *Phys. Rev. Lett.* **84**, 147–150 (2000).
29. De Wilde, Y. *et al.* Unusual strong-effects in the tunneling spectroscopy of optimally doped and overdoped $\text{Bi}_2\text{Sr}_2\text{CaCu}_2\text{O}_8$. *Phys. Rev. Lett.* **80**, 153–156 (1998).

Acknowledgements

We thank N. Nagaosa, D. J. Scalapino, R. Laughlin, D.-H. Lee, S. Kivelson, D. Bonn, K. A. Muller, P. Allen, N. P. Armitage, A. Damascelli and F. Ronning for discussions. The work at ALS and SSRL was supported by the Department of Energy’s Office of Basic Energy Science, Division of Materials Science. The Stanford work was also supported by the NSF. A.L. thanks the Instituto Nazionale Fisica della Materia (INFM) and the University of Rome “La Sapienza” for support.

Correspondence and requests for materials should be addressed to: Z.-X.S. (e-mail: zxshen@stanford.edu).

Fragile-to-strong transition and polyamorphism in the energy landscape of liquid silica

Ivan Saika-Voivod*, Peter H. Poole* & Francesco Sciortino†

* Department of Applied Mathematics, University of Western Ontario, London, Ontario N6A 5B7, Canada

† Dipartimento di Fisica and Istituto Nazionale per la Fisica della Materia, Università di Roma La Sapienza, Piazzale Aldo Moro 2, I-00185, Rome, Italy

Liquid silica is the archetypal glass former, and compounds based on silica are ubiquitous as natural and man-made amorphous materials. Liquid silica is also the extreme case of a ‘strong’ liquid, in that the variation of viscosity with temperature closely follows the Arrhenius law as the liquid is cooled toward its glass transition temperature^{1,2}. In contrast, most liquids are to some degree ‘fragile’, showing significantly faster increases in their viscosity as the glass transition temperature is approached. Recent studies^{3–6,35,36} have demonstrated the controlling influence of the potential energy hypersurface (or ‘energy landscape’) of the liquid on the transport properties near the glass transition. But the origin of strong liquid behaviour in terms of the energy landscape has not yet been resolved. Here we study the static

and dynamic properties of liquid silica over a wide range of temperature and density using computer simulations. The results reveal a change in the energy landscape with decreasing temperature, which underlies a transition from a fragile liquid at high temperature to a strong liquid at low temperature. We also show that a specific heat anomaly is associated with this fragile-to-strong transition, and suggest that this anomaly is related to the polyamorphic behaviour of amorphous solid silica.

In a molecular dynamics computer simulation of an equilibrium liquid, the diffusion coefficient D is readily evaluated from the particle trajectories. Like the viscosity, D is a characteristic transport property whose deviations from the Arrhenius law serve to classify a liquid as strong or fragile. The theory of Adam and Gibbs (AG)⁷ states that D is related to the configurational entropy, S_c through

$$D = D_0 \exp(-A/TS_c) \tag{1}$$

where the parameters D_0 and A are commonly assumed to be independent of temperature, T . The entropy S_c quantifies the number of distinct configurational states explored by the liquid in equilibrium. It has been suggested that these states correspond to the ‘basins’ of the potential energy hypersurface (PES) sampled by the liquid^{8,9}. A basin is the set of points in phase space representing configurations having the same local minimum. The local minimum configuration is termed an inherent structure (IS), and is identified in simulation by a steepest descent minimization of the potential energy.

Following the thermodynamic formalism of Stillinger and Weber⁸, we can express the internal energy of the liquid as $E = e_{IS} + E_{\text{harm}} + E_{\text{anh}}$, where e_{IS} is the average inherent structure energy and the last two terms are the average contributions to E due to thermal excitations about the IS. The term E_{harm} is the average harmonic contribution determined from a quadratic approximation to E around each inherent structure minimum, and E_{anh} is the remaining, necessarily anharmonic contribution. The harmonic and anharmonic potentials characterize the shape of the basin.

If the shape of the basins does not depend on e_{IS} (a condition

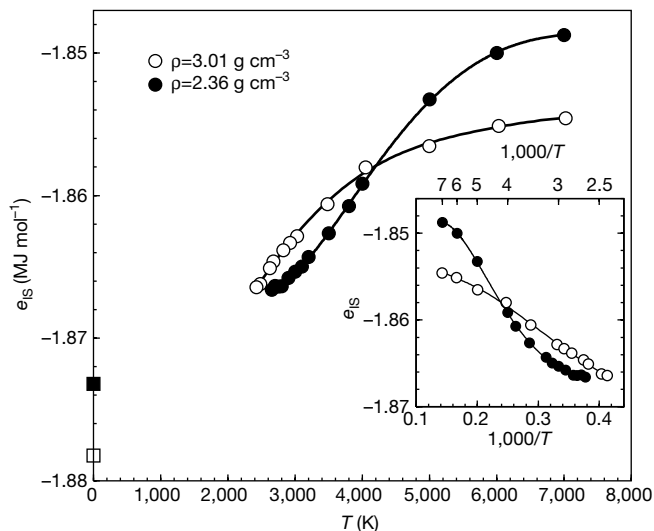


Figure 1 Variation of inherent structure energy e_{IS} with temperature T . Main panel: e_{IS} as a function of T along two isochores. At $T = 0$ we show the energy E_0 of the crystalline system at density $\rho = 2.36 \text{ g cm}^{-3}$ (filled square) and $\rho = 3.01 \text{ g cm}^{-3}$ (open square). E_0 is found by calculating the volume dependence of the potential energy at $T = 0$ of three crystal polymorphs of silica (stishovite, coesite and quartz), and then using the common tangent construction to determine the potential energy of the heterophase of coexisting crystals that would be the ground state at the required bulk value of ρ . Inset: e_{IS} for the same isochores as in the main panel, plotted as a function of $1/T$. Only the high-density data show a clear $1/T$ behaviour at low T .

satisfied at constant density ρ in the present study; see Methods), then S_c can be calculated along an isochore by integrating the T dependence of e_{IS} at constant volume V (ref. 3):

$$S_c = S_c^0 + \int_{T_0}^T \frac{1}{T'} \left(\frac{\partial e_{IS}}{\partial T'} \right)_V dT' \quad (2)$$

where S_c^0 is the value of S_c at a reference temperature $T = T_0$ (see Methods). Equation (2) highlights that the T dependence of S_c arises solely from changes in e_{IS} (refs 3, 8). Evaluation of S_c when the basin shape depends on e_{IS} is also feasible^{5,10,11}.

Some analyses of experimental data for silica suggest^{12,13} that the liquid may be fragile at very high T , and recent simulations^{14,15} of the BKS model of silica¹⁶ support this possibility. Simulations conducted between temperatures of 2,750 and 6,000 K have shown that at the onset of slow dynamics, as reflected for example by the presence of two-step relaxation in structural autocorrelation functions, BKS silica is a fragile liquid. At about 3,300 K BKS silica transforms to a strong liquid and the T dependence of all characteristic relaxation times follows the Arrhenius law¹⁵.

The relationship of such a ‘fragile-to-strong’ transition to the PES is not yet known. For a strong liquid that satisfies equation (1) the T dependence of S_c must approach a constant to recover Arrhenius behaviour. From equation (2), if S_c is constant, then so must be the variation of e_{IS} with T . This behaviour would be qualitatively different from that found in simulations of fragile liquids. For example, recent studies of a binary Lennard-Jones liquid have shown that e_{IS} is proportional to $-1/T$, a dependence consistent with a gaussian distribution of IS energies^{4,5}. When the distribution of inherent structure energy is gaussian, fragility has been shown to depend on the total number of IS states, the width of the gaussian, and the variation of the basin shape with e_{IS} (refs 5, 17). It is not known, however, if the PES of a liquid exhibiting a fragile-to-strong crossover is similarly characterized by a gaussian distribution of inherent structure energies but with parameters that differ from those of the fragile liquid, or if the PES is qualitatively different from that of a fragile liquid.

To address these questions, we conduct extensive equilibrium simulations of BKS silica over a large range of T and ρ to examine the fragile-to-strong transition, and to identify the energy landscape behaviour that underlies it. The results clarify our understanding both of the origins of silica’s status as a strong liquid, and of the dynamical behaviour of a wider class of liquids that are to some degree silica-like, most notably water and silicon (S. Sastry, personal

communication), but also other systems such as BeF_2 (ref. 18). Indeed, the concept of a ‘fragile-to-strong’ transition was first proposed for the case of deeply supercooled water¹⁹.

Figure 1 shows the T dependence of e_{IS} along two isochores. The shape of the higher ρ isochore is similar to that found for fragile liquids. But at the lower ρ —which is close to the experimental ρ at ambient pressure— e_{IS} shows an inflection, passing from concave downwards at high T to concave upwards at low T . Figure 1 also shows the potential energy E_0 at $T = 0$ of the corresponding equilibrium crystalline system for the same ρ . As the energy of the lowest IS cannot be less than E_0 , E_0 sets a lower bound on e_{IS} . The value of E_0 relative to the measured e_{IS} curves confirms that an inflection occurs.

The inset of Fig. 1 shows that the relation $e_{IS} \propto -1/T$, the hallmark of a gaussian distribution of IS energies, is not obeyed along our lower ρ isochore. The breakdown of this relation does not arise from changes in the shapes of the basins sampled at different T . Indeed, we find that at constant ρ , the harmonic contribution to the vibrational entropy does not depend on the basin depth; our results are also consistent with the anharmonic contribution to the vibrational entropy being independent of basin depth (see Methods).

Like e_{IS} , S_c also has an inflection along our lower ρ isochore (Fig. 2). Our S_c data thus reveal the signature in the energy landscape of a fragile-to-strong transition. The rapid variation of landscape properties at high T corresponds to a fragile regime. As T decreases, the inflections of e_{IS} and S_c mark the onset of a regime in which the rate of change of these quantities decreases, consistent with the system’s approach to the strong liquid limit.

In the range of T near the inflections of e_{IS} and S_c , we find (Fig. 3) that along both the high and low ρ isochores, D satisfies the AG relation within numerical error. That is, whether or not there is a change in the nature of the T dependence of S_c , the transport properties of the liquid adjust so as to maintain the AG relation, a finding that demonstrates the robustness of equation (1) (refs 5, 20, 21). As in simulations of binary Lennard-Jones liquids⁵ and water²¹, we also find that the slope of the isochores in Fig. 3 varies with ρ ; understanding this dependence is an important open question in the study of liquid dynamics using the PES.

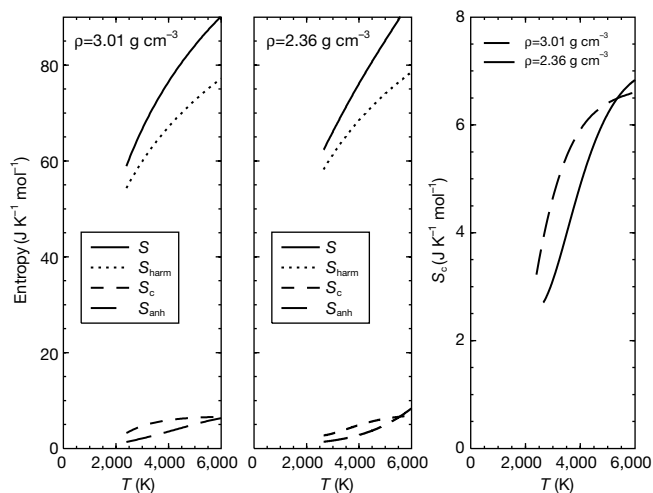


Figure 2 Entropy S and its component contributions as a function of temperature. Shown are isochores for $\rho = 3.01 \text{ g cm}^{-3}$ (left panel) and $\rho = 2.36 \text{ g cm}^{-3}$ (centre panel), and the configurational entropy S_c as a function of T along two isochores (right panel).

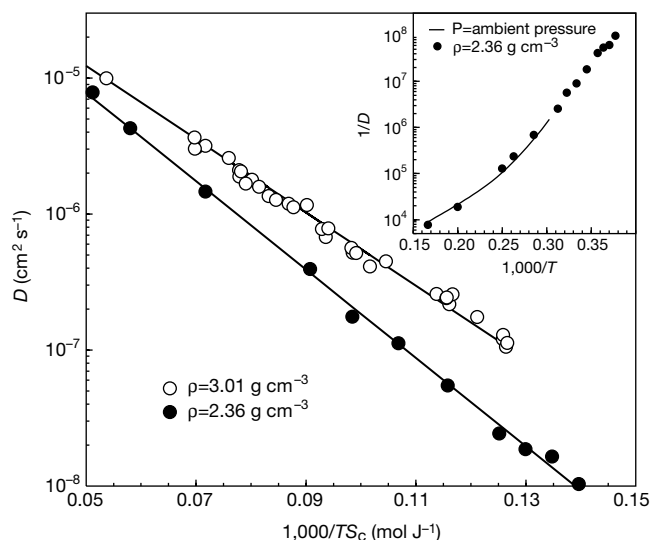


Figure 3 Relationship of diffusion coefficient D to temperature T and configurational entropy S_c . Main panel: $\log D$ versus $1/TS_c$ along two isochores. Inset: Arrhenius plot of $1/D$ along the ambient pressure isobar, found by interpolating our isochoric data; and along the $\rho = 2.36 \text{ g cm}^{-3}$ isochore. Note the crossover from non-Arrhenius to Arrhenius behaviour observed both at constant ρ and at constant pressure, P . All D values reported here are for Si atoms.

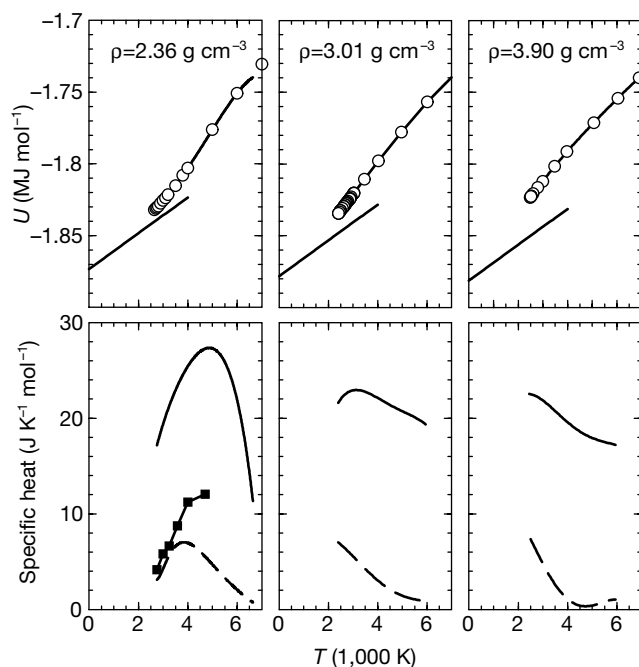


Figure 4 Potential energy U and isochoric specific heat C_V as a function of T . Upper panels: isochores of U . Lower panels: $C_V - (3/2)R$ (solid lines) and C_V^S (dashed lines) as a function of T . In the upper panels are shown lines of slope $\frac{3}{2}R$ whose values at $T = 0$ are the potential energies of the corresponding crystalline systems, calculated as described in

Fig. 1; these lines are lower bounds for U of the liquid. In the left-most lower panel are shown (filled squares) estimates of the configurational part of C_V recently evaluated by Scheidler *et al.*³⁴, calculated from the time dependence of the temperature fluctuations.

We note that for the present model, S_c is much smaller than the vibrational entropy ($S_{\text{harm}} + S_{\text{anh}}$) and of the same order as S_{anh} . Moreover, we find that for BKS silica the crystalline vibrational entropy differs significantly from the liquid vibrational entropy, as also found by Richet² in his extensive analysis of silicate melts. This confirms that for silica, the identification of the excess entropy (liquid entropy minus crystal entropy) with S_c may not be adequate^{22,23}. This highlights the value of finding S_c by the ‘all-liquid route’²⁴ used here. We also note that estimates of the configurational entropy (expressed in the units used here) of a random tetrahedral network range from 0.83 to 1.94 $\text{J K}^{-1} \text{mol}^{-1}$ (refs 25, 26). These estimates are consistent with our calculations, in that our S_c data are plausibly approaching this range from above at low T .

The influence of the energy landscape is sufficiently prominent to appear in the total thermodynamic properties²⁷. The isochoric specific heat C_V can be written as $C_V = C_V^{\text{IS}} + 3R + C_V^{\text{anh}}$, where each term is the derivative with respect to T of the corresponding contribution to E , and R is the gas constant. The inflection in the T dependence of e_{IS} corresponds to a maximum in C_V^{IS} (Fig. 4) that is the origin of a C_V anomaly, in the form of a peak, in the interval of T corresponding to the fragile-to-strong transition. An analogous C_V anomaly has recently been predicted to occur in the silica-like liquid BeF_2 (ref. 18), and in theoretical models designed to reproduce a fragile-to-strong transition²⁸. High- T experiments that test for this anomaly, although challenging, can thus directly seek the thermodynamic signature of the fragile-to-strong transition in these systems.

The peak that we find in C_V occurs at T near the temperature of maximum density of BKS silica, and near a maximum of the isothermal compressibility K_T predicted for this model²⁹. This interrelated set of liquid-state thermodynamic anomalies^{30,31} has been associated with the physics of polyamorphism in glasses—in other words, the rapid pressure-induced crossover of a low-density glass to a high-density glass³². Polyamorphism is observed experimentally during compression of silica glass, and the C_V maximum

found here may be the thermal anomaly corresponding to polyamorphism’s mechanical anomaly. Along different isochores we find that the T at which the C_V maximum occurs decreases with increasing ρ , as would be expected for an anomaly related to polyamorphism in silica. The maxima of C_V and K_T demarcate a zone of a rapid, but continuous, crossover in the thermodynamic properties of the liquid. In BKS silica, there is evidence²⁹ that this crossover becomes at lower T a discontinuous liquid–liquid phase transition. Although it is conceivable that such a first-order phase transition develops in real silica under appropriate conditions of temperature and pressure, the phase transition may be pre-empted by the glass transition, rendering it unobservable as a liquid-state phenomenon.

Consideration of the combined behaviour that we find for dynamic and thermodynamic properties suggests that the fragile-to-strong transition is the dynamical transition corresponding to the thermodynamic crossover in the liquid that presages polyamorphism²⁸. More generally, our results provide a basis for considering all strong liquids as candidates for polyamorphism: a strong liquid arises through a fragile-to-strong transition, associated with which may be thermodynamic anomalies that are the liquid-state precursors to polyamorphism. □

Methods

Computer simulations

Results are based on molecular dynamics simulations of BKS silica. All data are obtained from systems of $N = 1,332$ atoms (888 O and 444 Si atoms), except for the $\rho = 2.36 \text{ g cm}^{-3}$ isochore, where we use 999 atoms to achieve equilibration more easily at low T . At $\rho = 2.36 \text{ g cm}^{-3}$, eight independent runs for each state point are made. All data reported here are for liquid states in equilibrium. Equilibration is confirmed by ensuring that runs are longer than the slowest relaxation time in the system as evaluated from the collective (coherent) density–density correlation function. The lowest- T runs exceed 80 ns. Simulations are carried out in the constant- (N, V, E) ensemble, and long-range electrostatic interactions are accounted for by Ewald summation. We evaluate e_{IS} by conducting conjugate gradient minimizations of up to 1,000 equilibrium liquid configurations and averaging the results. Note that our thermodynamic results are reported per mole of atoms, rather than per mole of SiO_2 molecules.

Evaluation of the total entropy

For a given ρ , S at $T = T_0 = 4,000$ K is calculated using thermodynamic integration. We first find the free energy difference between an ideal gas and a binary mixture Lennard-Jones (LJ) system at the chosen ρ by integrating the excess pressure along an isotherm from the high- V limit where the system behaves as an ideal gas. We then carry out a set of simulations at constant V and T that continuously convert the LJ system to BKS silica, by using a hybrid potential $\phi = \lambda\phi_{\text{BKS}} + (1 - \lambda)\phi_{\text{LJ}}$ (ref. 33). An appropriate thermodynamic integration from $\lambda = 0$ to 1 yields the free energy of BKS silica, from which S at T_0 and the chosen ρ is calculated. The value of S at other temperatures is found by further thermodynamic integration at constant V .

Evaluation of the vibrational entropy

We evaluate S_{harm} from the spectrum of eigenfrequencies ν (that is, the vibrational density of states) calculated from the inherent structures at each T , using $S_{\text{harm}} = k\Sigma_{\nu=1}^{3N} [1 - \log(h\nu/kT)]$, where k and h are Boltzmann's and Planck's constants, respectively. To obtain S_{anh} we use E_{anh} . We evaluate $E_{\text{anh}} = E - E_{\text{harm}} - e_{\text{IS}}$ and then fit E_{anh} with a polynomial constrained to be zero and have zero slope at $T = 0$. Assuming that the shapes of the basins do not depend on e_{IS} , S_{anh} may be calculated by thermodynamic integration using the fitted form of E_{anh} from $T = 0$ to the desired T . In terms of the above quantities, the integration constant in equation (2) is thus $S_0^e = S(T_0) - S_{\text{anh}}(T_0) - S_{\text{harm}}(T_0)$.

Isochoric invariance of basin shape

Our assumption that the shape of the basins is independent of e_{IS} along an isochore is based on two observations. First we find that the vibrational density of states (the ν spectrum), is independent of e_{IS} along an isochore. Second, the anharmonic energy of inherent structure configurations heated from $T = 0$ to a chosen T follows the $E_{\text{anh}} = E - E_{\text{harm}} - e_{\text{IS}}$ curve calculated from equilibrium simulations. This is only possible if the anharmonic character of the basins is also to a large extent independent of e_{IS} .

Received 12 April; accepted 18 June 2001.

1. Angell, C. A. Relaxation in liquids, polymers and plastic crystals—Strong/fragile patterns and problems. *J. Non-Cryst. Solids* **131–133**, 13–31 (1991).
2. Richet, P. Viscosity and configurational entropy of silicate melts. *Geochim. Cosmochim. Acta* **48**, 471–483 (1984).
3. Sciortino, F., Kob, W. & Tartaglia, P. Inherent structure entropy of supercooled liquids. *Phys. Rev. Lett.* **83**, 3214–3217 (1999).
4. Buechner, S. & Heuer, A. The potential energy landscape of a model glass former: thermodynamics, anharmonicities, and finite size effects. *Phys. Rev. E* **60**, 6507–6518 (1999).
5. Sastry, S. The relationship between fragility, configurational entropy and the potential energy landscape of glass-forming liquids. *Nature* **409**, 164–167 (2001).
6. Martinez, L.-M. & Angell, C. A. A thermodynamic connection to the fragility of glass-forming liquids. *Nature* **410**, 663–667 (2001).
7. Adam, G. & Gibbs, J. H. On the temperature dependence of cooperative relaxation properties in glass-forming liquids. *J. Chem. Phys.* **43**, 139–146 (1965).
8. Stillinger, F. H. & Weber, T. A. Packing structures and transitions in liquids and solids. *Science* **225**, 983–989 (1984).
9. Stillinger, F. H. A topographic view of supercooled liquids and glass formation. *Science* **267**, 1935–1939 (1995).
10. Sciortino, F. & Tartaglia, P. Extension of the fluctuation-dissipation theorem to the physical aging of a model glass-forming liquid. *Phys. Rev. Lett.* **86**, 107–111 (2001).
11. Starr, F. W., Sastry, S., La Nave, E., Scala, S., Stanley, H. E. & Sciortino, F. Thermodynamic and structural aspects of the potential energy surface of simulated water. *Phys. Rev. E* **63**, 041201 (2001).
12. Rossler, E., Hess, K.-U. & Novikov, V. N. Universal representation of viscosity in glass forming liquids. *J. Non-Cryst. Solids* **223**, 207–222 (1998).
13. Hess, K.-U., Dingwell, D. B. & Rossler, E. Parametrization of viscosity-temperature relations of aluminosilicate melts. *Chem. Geol.* **128**, 155–163 (1996).
14. Barrat, J.-L., Badro, J. & Gillet, P. A strong to fragile transition in a model of liquid silica. *Molecular Simulation* **20**, 17–25 (1997).
15. Horbach, J. & Kob, W. Static and dynamic properties of a viscous silica melt. *Phys. Rev. B* **60**, 3169–3181 (1999).
16. Van Beest, B. W. H., Kramer, G. J. & van Santen, R. A. Force fields for silicas and aluminophosphates based on ab initio calculations. *Phys. Rev. Lett.* **64**, 1955–1958 (1990).
17. Speedy, R. J. Relations between a liquid and its glasses. *J. Phys. Chem. B* **103**, 4060–4065 (1999).
18. Hemmati, M., Moynihan, C. T. & Angell, C. A. Density maxima and minima, and water-like heat capacity and transport anomalies, in liquid BeF₂. *J. Chem. Phys.* (in the press).
19. Angell, C. A. Water II is a strong liquid. *J. Phys. Chem.* **97**, 6339–6341 (1993).
20. Speedy, R. J. The hard sphere glass transition. *Mol. Phys.* **95**, 169–178 (1998).
21. Scala, A., Starr, F. W., La Nave, E., Sciortino, F. & Stanley, H. E. Configurational entropy and diffusivity of supercooled water. *Nature* **406**, 166–169 (2000).
22. Johari, G. P. Contributions to the entropy of a glass and liquid, and the dielectric relaxation time. *J. Chem. Phys.* **112**, 7518–7523 (2000).
23. Goldstein, M. Viscous liquids and the glass transition: sources of the excess heat capacity. *J. Chem. Phys.* **51**, 3728–3739 (1969).
24. Coluzzi, B., Parisi, G. & Verrocchio, P. Thermodynamical liquid-glass transition in a Lennard-Jones binary mixture. *Phys. Rev. Lett.* **84**, 306–309 (2000).
25. Bell, R. J. & Dean, P. The configurational entropy of vitreous silica in the random network theory. *Phys. Chem. Glasses* **9**, 125–127 (1968).
26. Speedy, R. J. & Debenedetti, P. G. The distribution of tetravalent network glasses. *Mol. Phys.* **88**, 1293–1316 (1996).
27. Stillinger, F. H., Debenedetti, P. G. & Sastry, S. Resolving vibrational and inherent structural contributions to isothermal compressibility. *J. Chem. Phys.* **109**, 3983–3988 (1998).

28. Jagla, E. A. Fragile-strong transitions and polymorphism in glass forming fluids. *Mol. Phys.* **99**, 753–757 (2001).
29. Saika-Voivod, I., Sciortino, F. & Poole, P. H. Computer simulation of liquid silica: equation of state and liquid-liquid phase transition. *Phys. Rev. E* **63**, 011202 (2001).
30. Sastry, S., Debenedetti, P. G., Sciortino, F. & Stanley, H. E. Singularity-free interpretation of the thermodynamics of supercooled water. *Phys. Rev. E* **63**, 6144–6154 (1996).
31. Rebelo, L. P. N., Debenedetti, P. G. & Sastry, S. Singularity-free interpretation of the thermodynamics of supercooled water. II. Thermal and volumetric behavior. *J. Chem. Phys.* **109**, 626–633 (1998).
32. Poole, P. H., Grande, T., Angell, C. A. & McMillan, P. F. Polymorphic phase transitions in liquids and glasses. *Science* **275**, 322–323 (1997).
33. Mezei, M. & Beveridge, D. L. Free energy simulations. *Ann. NY Acad. Sci.* **482**, 1–23 (1986).
34. Scheidler, P., Kob, W., Latz, A., Horbach, J. & Binder, K. Frequency-dependent specific heat of silica. *Phys. Rev. B* **63**, 104204 (2001).
35. Sastry, S., Debenedetti, P. G. & Stillinger, F. H. Signatures of distinct dynamical regimes in the energy landscape of a glass-forming liquid. *Nature* **393**, 554–557 (1998).
36. Debenedetti, P. G. & Stillinger, F. H. Supercooled liquids and the glass transition. *Nature* **410**, 259–267 (2001).

Acknowledgements

We thank C. A. Angell, W. Kob, S. Sastry and R. Speedy for discussions. I.S.-V. and P.H.P. thank NSERC (Canada) for financial support, and SHARCNET for computing resources. E.S. acknowledges support from the INFN 'Iniziativa Calcolo Parallelo' and PRE-HOP and from MURST PRIN 2000.

Correspondence and requests for materials should be addressed to P.H.P. (e-mail: poole@cmrg.apmaths.uwo.ca).

Growth dynamics of pentacene thin films

Frank-J. Meyer zu Heringdorf, M. C. Reuter & R. M. Tromp

IBM T.J. Watson Research Center, Yorktown Heights, PO Box 218, New York 10598, USA

The recent demonstration of single-crystal organic optoelectronic devices has received widespread attention^{1–4}. But practical applications of such devices require the use of inexpensive organic films deposited on a wide variety of substrates. Unfortunately, the physical properties of these organic thin films do not compare favourably to those of single-crystal materials. Moreover, the basic physical principles governing organic thin-film growth and crystallization are not well understood. Here we report an *in situ* study of the evolution of pentacene thin films, utilizing the real-time imaging capabilities of photoelectron emission microscopy. By a combination of careful substrate preparation and surface energy control, we succeed in growing thin films with single-crystal grain sizes approaching 0.1 millimetre (a factor of 20–100 larger than previously achieved), which are large enough to fully contain a complete device. We find that organic thin-film growth closely mimics epitaxial growth of inorganic materials, and we expect that strategies and concepts developed for these inorganic systems will provide guidance for the further development and optimization of molecular thin-film devices.

'Plastic transistors' offer possibilities for flexible displays, and all-plastic smart cards and badges, as well as light-emitting diodes and lasers^{1,5–8}. Pentacene (C₁₄H₂₂), a chain-like aromatic molecule composed of five benzene rings, is among the most promising materials. Recent progress in organic electronics has focused on the exploration of new devices in single-crystal materials^{1–4,9}. However, electrical properties of polycrystalline films are inferior to those of single-crystal materials, and—because the mobility in single-crystal bulk material is higher⁵ than the values reported for organic thin-film transistors (OTFTs)—improvement of the film quality is mandatory¹⁰.